HHS Public Access

Author manuscript

Cancer Res. Author manuscript; available in PMC 2016 December 01.

Published in final edited form as:

Cancer Res. 2015 December 1; 75(23): 5058–5069. doi:10.1158/0008-5472.CAN-15-0744.

Fibulin-5 blocks microenvironmental ROS in pancreatic cancer

Miao Wang[1,*], **Mary Topalovski**[1,*], **Jason E. Toombs**[1], **Christopher M. Wright**[1], **Zachary R. Moore**[2], **David A. Boothman**[2], **Hiromi Yanagisawa**[3], **Huamin Wang**[6], **Agnieszka Witkiewicz**[4], **Diego H. Castrillon**[4], and **Rolf A. Brekken**[1,5,#]

[1]Hamon Center for Therapeutic Oncology Research, UT Southwestern Medical Center, 6000 Harry Hines Blvd., Dallas, TX 75390-8593, USA

[2]Simmons Comprehensive Cancer Center, UT Southwestern Medical Center, 6000 Harry Hines Blvd., Dallas, TX 75390-8593, USA

[3]Department of Molecular Biology, UT Southwestern Medical Center, 6000 Harry Hines Blvd., Dallas, TX 75390-8593, USA

[4]Department of Pathology, UT Southwestern Medical Center, 6000 Harry Hines Blvd., Dallas, TX 75390-8593, USA

[5]Departments of Surgery and Pharmacology, UT Southwestern Medical Center, 6000 Harry Hines Blvd., Dallas, TX 75390-8593, USA

[6]Department of Pathology, UT MD Anderson Cancer Center, Houston TX 77030, USA

Abstract

Elevated oxidative stress is an aberration seen in many solid tumors, and exploiting this biochemical difference has the potential to enhance the efficacy of anti-cancer agents. Homeostasis of reactive oxygen species (ROS) is important for normal cell function, but excessive production of ROS can result in cellular toxicity and therefore ROS levels must be balanced finely. Here, we highlight the relationship between the extracellular matrix and ROS production by reporting a novel function of the matricellular protein Fibulin-5 (Fbln5). We employed genetically engineered mouse models of pancreatic ductal adenocarcinoma (PDA) and found that mutation of the integrin-binding domain of Fbln5 led to decreased tumor growth, increased survival, and enhanced chemoresponse to standard PDA therapies. Through mechanistic investigations, we found that improved survival was due to increased levels of oxidative stress in Fbln5 mutant tumors. Furthermore, loss of the Fbln5-integrin interaction augmented fibronectin signaling, driving integrin-induced ROS production in a 5-lipooxygenase-dependent manner. These data indicate that Fbln5 promotes PDA progression by functioning as a molecular rheostat that modulates cell-ECM interactions to reduce ROS production and thus tip the balance in favor of tumor cell survival and treatment-refractory disease.

[#]Corresponding author: Rolf A. Brekken, PhD, Hamon Center for Therapeutic Oncology Research, University of Texas Southwestern Medical Center, 6000 Harry Hines Blvd., Dallas, TX 75390-8593, Tel: 214.648.5151; Fax: 214.648.4940 rolf.brekken@utsouthwestern.edu.

[*]These authors contributed equally to this work

Disclosure of Potential Conflicts of Interest: RA Brekken, co-founder of Tuevol Therapeutics, a company that is developing therapeutics that target the tumor microenvironment

Introduction

Tumors develop and progress in the context of the extracellular matrix (ECM). In fact, structural ECM proteins can promote tumor cell survival and stimulate invasive tumor cell programs (1-6). This is particularly evident in desmoplastic tumors, such as pancreatic ductal adenocarcinoma (PDA) (7), where ECM proteins including fibronectin (FN) and collagen activate signaling pathways that drive cell survival, proliferation and migration (1, 2). ECM-mediated signaling is governed by expression of the ECM proteins, the presence of cell surface receptors and the expression and activity of matricellular proteins that function as extracellular adaptors to reduce ECM-cell interaction (1, 8, 9). Fibulin-5 (Fbln5), a member of the fibulin family of proteins, is particularly important in this regard, as it binds to α4β1 and α5β1 integrins via an RGD sequence, but does not support integrin activation (8). Thus, Fbln5 competes with structural ECM ligands, principally FN, that would otherwise activate these integrins.

ECM proteins stimulate the generation of reactive oxygen species (ROS) in an integrin-dependent manner (2, 10, 11). ROS generation in this context is generally transient and serves primarily as a signaling intermediate that enhances cellular activity (12). We reasoned that a chronic increase in integrin-induced ROS would negatively affect tumor growth. FN-driven ROS generation is an attractive pathway to exploit for this strategy because FN ligation of β1 integrins is governed in part by Fbln5 (8, 13). We reported previously that Fbln5 reduced FN-mediated integrin-induced ROS production by competing with FN for binding to α5β1 integrin (13). Mutation of the three amino acid RGD sequence in Fbln5 to RGE abolishes integrin binding yet preserves other functions of Fbln5 (14, 15). An essential function of Fbln5 is elastic fiber formation (16). As a result, *Fbln5*$^{-/-}$ mice exhibit disorganized elastic fibers throughout the body leading to tortuous great vessels, emphysematous lungs and loose skin, resembling cutis laxa syndrome in humans (17, 18). In contrast, *Fbln5*$^{RGE/RGE}$ (*RGE*) mice have intact elastic fibers and are essentially indistinguishable from wild-type (*WT*) littermates (15). However, *RGE* mice show increased levels of ROS compared to *WT* animals in tissues where FN is abundant (15). Given the high expression of FN in the stroma of PDA and increasing evidence supporting enhanced ROS production as an anti-cancer strategy (19), we evaluated the consequence of ablating the integrin binding ability of Fbln5 in robust spontaneous models of PDA. Our results show that Fbln5-integrin interaction promotes aggressive tumor growth and progression in mice and that 5-lipooxygenase (5-LOX) activity was required for ROS induction in the absence of functional Fbln5. Additionally, we found that Fbln5 was expressed abundantly in the stroma of human PDA tumors. These data provide insight into the function of Fbln5 in PDA and reveal how ECM signaling might be exploited to drive pro-oxidant therapy.

Materials and Methods

Mouse models

Fbln5$^{RGE/RGE}$ (*RGE*), *Fbln5*$^{-/-}$ (*KO*), *LSL-Kras*$^{G12D/+}$; *Cdkn2a*$^{Lox/Lox}$ (*KI*) and *Cdkn2a*$^{Lox/Lox}$; *p48*^{Cre} (*IC*) mice were generated as previously described (1, 15, 45, 46). *RGE* mice were used to breed with *KI* and *IC* mice to generate genetically matched *LSL-Kras*$^{G12D/+}$; *Cdkn2a*$^{Lox/Lox}$; *p48*^{Cre} (*KIC*) mice and *RGE-KIC* mice. *LSL-Trp53*$^{R172H/+}$ mice

were obtained from National Cancer Institute (NCI) Mouse Repository (22). *RGE* mice were also used to breed with *LSL-Kras*$^{G12D/+}$; *LSL- Trp53*$^{R172H/+}$ (*KP*) and *p48*^{Cre} mice to generate genetically matched *LSL-Kras*$^{G12D/+}$; *LSL-Trp53*$^{R172H/+}$; *p48*^{Cre} (*KPC*) mice and *RGE-KPC* mice. All mice were housed in a pathogen-free facility and all experiments were performed under written protocols approved by the Institutional Animal Care and Use Committee at the University of Texas Southwestern (UTSW) Medical Center at Dallas.

Animal studies

For endpoint studies, *KIC* and *RGE-KIC* mice were sacrificed and entire tissues including pancreas/tumor, liver and spleen were harvested and weighed at 1, 1.5 and 2 months old. *KPC* and *RGE-KPC* mice were sacrificed at 3 and 5 months, n≥8 mice per time point per group. For all survival studies, mice were carefully monitored and sacrificed when they appeared moribund. For antioxidant treatment, N-acetyl cysteine (NAC) (Sigma Aldrich) was given to mice at 7 mg/ml in the drinking water from 4 weeks old until moribund. For endpoint therapy experiments, *KIC* and *RGE-KIC* mice were treated for 3 weeks starting at 7 weeks (1.5 months) of age with intraperitoneal (i.p.) injection of low dose Gemcitabine (GemL; 12.5 mg/kg 3×/week) or Abraxane (Abx; 5 mg/kg 2×/week). Mice were sacrificed and tissues were isolated for analysis, n ≥6 mice per group. For survival studies with therapy, cohorts of *KIC* and *RGE-KIC* mice were treated similarly with GemL, high dose Gemcitabine (GemH; 50 mg/kg 1×/week i.p.) or Abx until moribund.

Histology, immunohistochemistry (IHC) and immunofluorescence (IF) staining

Tissues were snap frozen and embedded in OCT (Tissue-Tek) for frozen sections or fixed with 4% paraformaldehyde (PFA) overnight and embedded in paraffin for sectioning. Frozen sections were fixed in ice-cold acetone for 5 minutes (min), air dried for 10 min followed by 10 min incubation with PBS to dissolve the OCT. Paraffin sections were deparaffinized and rehydrated with xylene and serial dilutions of ethanol followed by antigen retrieval with 0.01 M citric acid buffer (pH 6.0). Sections were blocked with 20% aquablock and incubated with primary antibodies in blocking solution (5% BSA in TBST) at 4°C overnight. Primary antibodies used for frozen sections were: rabbit polyclonal anti-mouse Fbln5 (1:100) (purified polyclonal IgG by our lab, 1.6 mg/ml) (17), rat anti-Meca32 (1:100) (purified IgG from hybridoma by our lab) (47), goat anti-Amylase (1:2000) (sc-12821, Santa Cruz Biotechnology), rabbit anti-fibronectin (1:100) (DP3060, Acris) and rabbit anti-γH2AX (1:50) (NB100-2280, NOVUS). Primary antibodies used for paraffin sections were: rabbit anti-human Fbln5 (1:75) (HPA000868, Sigma Aldrich), rabbit anti-Phospho-Histone H3 (PH3) (1:100) (06-570, Millipore), rabbit anti-Amylase (1:2000) (3796S, Cell Signaling) and rat anti-endomucin (1:100) (sc-65495, Santa Cruz Biotechnology). Fluorescein Isothiocyanate (FITC)-conjugated donkey anti-rabbit, rat IgGs, Cyanine 3 (Cy3)-conjugated donkey anti-rat, mouse, rabbit IgGs and Horseradish Peroxidase (HRP)-conjugated donkey anti-rabbit IgGs from Jackson ImmunoResearch were used as secondary antibodies.

Slides with sections of FFPE de-identified human pancreatic cancer tissue were obtained from the UT Southwestern Tissue Resource and the Department of Pathology, UT MD

Anderson Cancer Center. Human PDA sections were stained for Fbln5 expression using rabbit anti-Fbln5 (HPA000868, Sigma Aldrich) as indicated above.

Western blot analysis

Western blots were performed as previously described (49). In brief, protein lysates from cell culture or tumor tissues were extracted in ice-cold RIPA buffer (50 mM Tris-Cl, 150 mM NaCl, 1% NP-40, 0.5% sodium deoxycholate, 0.1% SDS) containing cocktails of protease (Thermo Scientific) and phosphatase inhibitors (Sigma-Aldrich), by centrifugation (13000g, 15 min) at 4°C following 3 freeze-thaw cycles. Proteins were separated by SDS-PAGE and transferred to methanol activated polyvinylidene difluoride (PVDF) membrane (VWR). The primary antibodies used include the following: rabbit anti-mouse Fbln5 (1:1000), rabbit anti-human Fbln5 (1:500) (HPA000868, Sigma Aldrich), anti-Nqo1 (1:1000) (ab34173, Abcam), anti-α-Tubulin (1:1000) (ab4047, Abcam) and anti-β-actin (1:5000) (A2066, Sigma-Aldrich). HRP-conjugated donkey anti-rabbit IgG (1:10000) (Jackson Immunoresearch) as secondary antibodies were used.

Cell culture

Cell lines used include mouse endothelial cell line bEnd.3 (13), mouse pancreatic cancer cell lines Pan02 (13) and mPLR B9 (1), and human pancreatic cell lines MiaPaCa-2, AsPC-1 and Panc1 (all purchased from ATCC). NG2+ cells were isolated using anti-NG2 antibody conjugated magnetic beads from a *KIC* tumor (50). *Fbln5*$^{+/+}$ (WT), *Fbln5*$^{-/-}$ (*KO*) and *Fbln5*$^{RGE/RGE}$ (*RGE*) mouse embryonic fibroblasts (MEFs) were isolated from embryonic day E12.5-E14.5 embryos and genotypes were confirmed by PCR. bEnd.3 cells were treated with 100 μM H_2O_2 or 10 μg/ml α5β1 integrin activating antibody and lysates were collected for Western blot analysis. MEFs were cultured in reduced serum medium Opti-MEM (Life Technologies) overnight before being plated on plastic, FN (Sigma Aldrich) or collagen I (Fisher Scientific), each at 10 μg/ml unless otherwise noted. After plating, MEFs were grown in serum free medium (SFM) supplemented with FN, collagen, β1 integrin blocking antibody (each at 10 μg/ml) or various chemicals. Inhibitors used for various ROS sources include Rotenone (R8875-1G, Sigma Aldrich), Diphenyleneiodonium chloride (DPI) (D2926, Sigma-Aldrich) and nordihydroguaiaretic acid (NDGA) (479975, Millipore). All cells were maintained in Dulbecco's modified Eagle's medium (DMEM) (Mediatech, Inc.) with 10% fetal bovine serum (FBS) and were grown in 37°C humidified incubator with 5% CO_2. MEFs were used between passages 2-5 for all experiments.

ROS detection

The detailed protocol on ROS detection and quantification has been described previously (13). In brief, for tissues, 5 μM dihydroethidium (DHE) (D11347, Life technologies) was applied to freshly sectioned tissues and incubated at 37°C for 30 minutes. 6-10 images were taken randomly from each tissue and at least 3 tissues were included in each group. Fluorescence intensity was quantified by the software NIS-Elements. To visualize ROS in cells, 10 μM of 2′-7′-dicholordihydrofluorescein diacetate (DCF-DA) (D-399, Life Technologies) was added to cells grown on fibronectin (FN)-coated chamber slides. 8-10 pictures were taken randomly from each condition and area fraction was quantified and

normalized to cell number by DAPI using the software NIS-Elements. Three independent experiments for each condition were evaluated.

qPCR array and Real-time PCR

WT and *RGE* MEFs were cultured in reduced serum medium Opti-MEM overnight before plating on FN. Upon plating, MEFs were grown in serum free medium (SFM) supplemented with FN for 4, 16 and 24 hrs. RNA lysates were isolated using RNeasy plus mini kit (Qiagen). RT^2 first strand kit (Qiagen) was used for cDNA synthesis. Then cDNA samples were subjected to RT^2 Profiler™ PCR array to analyze gene expression changes related to mouse oxidative stress and antioxidant defense pathways (Qiagen, PAMM-065A). Experiments were performed and data were analyzed following manufacturer's instructions. All the candidate genes were further checked and confirmed by Real-time PCR. Ribosome protein S6 (RPS6) was used as the internal control. Following primers were used for real-time PCR: Nqo1 (forward): 5′-AGACCTGGTGATATTTCAGTTCCCATTG-3′; Nqo1 (reverse): 5′-CAAGGTCTTCTTATTCTGGAAAGGACCGT-3′; RPS6 (forward): 5′-AAGCTCCGCACCTTCTAT-3′; RPS6R (reverse) :5′-TGACTGGACTCAGACTTAGAAGTAGAAGC-3′.

Nqo1 activity assay

Nqo1 enzyme activity was measured in a reaction mixture containing 200 μM NADH (Sigma Aldrich) as an electron donor and 10 μM menadione (Sigma Aldrich) as an Nqo1 substrate and intermediate electron acceptor as described (51, 52). Cytochrome c serves as the terminal electron acceptor. Therefore, the measured rate of cytochrome c reduction correlates with Nqo1 enzymatic activity. To prepare lysates, cells were scraped in PBS and samples were sonicated. Lysate was added to the reaction mixture and the reduction of cytochrome c (Sigma Aldrich) over two minutes was monitored by absorbance at 550 nm. Dicoumarol, a selective inhibitor of Nqo1, was added as a negative control. Enzyme activity units were calculated as nmol of cytochrome c reduced/min/μg lysate.

Statistical analysis

For statistical analysis, unpaired *t*-test was used for comparison between genotypes and various groups. Log-rank (Mantel-Cox) test was used for all the mouse survival studies. Overall, *P* value less than 0.05 was considered as statistically significant. *, $p<0.05$; **, $p<0.01$; ***, $p<0.001$; ****, $p<0.0001$.

Results

Fbln5 expression in pancreatic cancer

The expression of Fbln5 is prominent in developing arteries and is diminished in most adult organs, but can be reactivated in injured vessels (14). We examined Fbln5 expression in multiple mouse and human cell lines and tumor lysates. The mouse endothelial cell line bEnd.3 and fibroblasts, including mouse embryo fibroblasts (MEFs) and fibroblasts isolated from mouse PDA ($NG2^+$ cells), expressed Fbln5 (Fig. 1A and S1B) as did human and mouse PDA lysates (Fig. 1B and S1C). In contrast, pancreatic cancer cell lines including three human (MiaPaCa-2, Panc1 and AsPC-1) (Fig. 1B) and four mouse lines (Pan02 and

three isogenic lines isolated from mouse PDA) did not express detectable levels of Fbln5 protein (Fig. 1A, S1B and data not shown). However, all cell lines and PDA tumor lysates examined express α5β1 integrin (Fig. S1A and S1C), which serves as the cell surface receptor for Fbln5 and FN (8).

Fbln5 immunohistochemistry (IHC) in syngenic pancreatic Pan02 tumors grown subcutaneously in *Fbln5*$^{+/+}$ (WT) or *Fbln5*$^{-/-}$ (KO) mice revealed that Fbln5 is produced by stromal cells (Fig. 1E). Co-staining of Fbln5 with the endothelial cell marker Meca32 shows that Fbln5 can be produced by endothelial cells within the tumor (Fig. 1E). IHC analysis of Fbln5 expression in multiple mouse models of PDA revealed Fbln5 reactivity mainly in the stroma (Fig. 1C-D and data not shown). We also examined FBLN5 in human PDA by IHC and found the protein was expressed in all human PDAs examined (n=25). The staining pattern was confined largely to the stromal compartment; however, not all regions of stroma were positive for FBLN5 protein (Fig. 1F). The nature of the heterogeneous stromal staining pattern is unclear but suggests that FBLN5 expression is controlled tightly.

Characterization of *KIC* and *KPC* mice

To evaluate the contribution of Fbln5 to PDA development and progression we utilized *KIC* and *KPC* mice, two well established conditional genetically engineered mouse models (GEMMs) of PDA based on the p48^{Cre} (also known as Ptf1a) driver, which is expressed in pancreatic bud progenitor cells (20-22). *KIC* animals express an active form of *Kras* and have biallelic inactivation of the *Cdkn2a* locus (*LSL-Kras*$^{G12D/+}$; *Cdkn2a*$^{Lox/Lox}$; *p48*^{Cre}) (21). *KPC* animals express the same activating G12D mutation in *Kras* and also harbor a R172H point mutation in *p53*, the Li-Fraumeni human ortholog (*LSL-Kras*$^{G12D/+}$; *LSL-Trp53*$^{R172H/+}$; *p48*^{Cre}) (22). Histological examination of *KIC* and *KPC* pancreatic tissue by a pathologist revealed that each model developed early pancreatic intraepithelial neoplasias (PanINs) and highly infiltrative adenocarcinomas ranging from well-differentiated areas with clear malignant gland formation to areas that were more poorly differentiated (Fig. S2A). Similar to human PDA, Masson's trichrome staining showed extensive collagen deposition in the area of PanINs and PDA in *KIC* and *KPC* tumors (Fig. S2B).

Ablation of Fbln5-integrin interaction reduces tumor growth and prolongs survival

Mutation of the Fbln5 integrin binding sequence from RGD to RGE renders the protein incapable of binding to integrins (14). *Fbln5*$^{RGE/RGE}$ (*RGE*) mice are viable, fertile and phenotypically normal compared to *WT* animals (15). To study the contribution of Fbln5 to PDA development, we crossed *RGE* mice with *KIC* or *KPC* animals to generate genetically matched *KIC* and *RGE-KIC*, *KPC* and *RGE-KPC* mice. There was no difference in Fbln5 expression levels between *KIC* and *RGE-KIC* or *KPC* and *RGE-KPC* tumors (Fig. 1G and S1D). However, tumors had significantly increased Fbln5 expression compared to normal pancreas (Fig. 1C, 1G and S1D). Pancreatic and mouse body weights were determined in *KIC* and *RGE-KIC* mice at 1, 1.5 and 2 months (Fig. S2C and 2A). There is no significant difference for tumor/body weight at 1 and 1.5 months (Fig. S2C). *RGE-KIC* mice exhibited significantly lower tumor/body weight at 2 months than *KIC* mice, with tumor weights ranging from 0.24 to 0.86 gram for *RGE-KIC* mice and 0.72 to 1.11 gram for *KIC* mice (Fig. 2A). This is consistent with significantly reduced proliferating cells in *RGE-KIC* tumors

(Fig. 2C-D). Similar results were observed in the *KPC* model, which were analyzed at 3 and 5 months of age (Fig. 2B and 2E-F).

Survival analysis revealed that *RGE-KIC* mice lived significantly longer than *KIC* mice (Fig. 2G) with a median survival of 74 days for *RGE-KIC* mice and 61.5 days for *KIC* mice. *KIC* and *RGE-KIC* mice appeared normal with no obvious phenotype up to 1.5 months of age but later became moribund, usually accompanied by weight loss. Moreover, some mice developed jaundice or ascites. Autopsies revealed the presence of large solid tumors with limited gross metastases. Liver micrometastasis was seen in the majority of *KIC* and *RGE-KIC* mice in the survival study necropsies (Fig. S2D). Similarly, *RGE-KPC* show significantly prolonged survival compared to *KPC* mice (175 days vs 143.5 days) (Fig. 2H). *KPC* and *RGE-KPC* mice appeared healthy up to 3 month old and were sacrificed between 3 to 9 months, commonly presenting with body weight loss, jaundice or ascites. Gross liver metastasis was seen in 30-40% of animals (Fig. S2E-F).

Increased oxidative stress in *RGE-KIC* and *RGE-KPC* tumors

We reported previously that the growth of subcutaneous Pan02 tumors in *Fbln5*$^{-/-}$ mice was significantly reduced compared to *WT* animals due to increased ROS (13). Dihydroethidium (DHE) staining of tumors from the GEMMs showed that the Fbln5 *RGE* mutation significantly induced ROS levels in *KIC* and *KPC* tumors (Fig. 3A-B). Accordingly, the level of γH2AX, a commonly used marker for oxidative stress-induced DNA damage (23), was higher in *RGE-KIC* tumors than *KIC* tumors (Fig. 3C). However, in the context of normal pancreatic tissue, the Fbln5 *RGE* mutation did not alter ROS levels (Fig. S3A-B). This is consistent with the level of FN expression, which was elevated in PDA compared to normal pancreatic tissue (Fig. 1H). To determine whether ROS induction contributed to the prolonged survival in *RGE* animals, *KIC* and *RGE-KIC* mice were treated with the antioxidant N-acetylcysteine (NAC) and survival was examined (Fig. 3D). Prolonged NAC treatment decreased survival of *RGE-KIC* mice but did not affect the survival of *KIC* mice (Fig. 3D). ROS production was also examined in NAC-treated *KIC* and *RGE-KIC* tumors, which revealed no difference between the two groups (Fig. S3C-D). Collectively, ROS induction driven by the Fbln5 *RGE* mutation resulted in reduced tumor growth and prolonged survival.

Angiogenesis is reduced in *RGE-KIC* and *RGE-KPC* tumors

Prior studies indicate that Fbln5 can modulate angiogenesis (24) and we reported that loss of Fbln5 resulted in decreased angiogenesis in pancreatic tumors (13). Therefore, we examined microvessel density (MVD) in *KIC* and *RGE-KIC*, *KPC* and *RGE-KPC* tumors by co-immunostaining with the endothelial cell marker endomucin and the acinar cell marker amylase. MVD was significantly reduced in *RGE-KIC* compared to *KIC* in tumor regions as marked by loss of amylase reactivity (Fig. 3E-F and S4A). Immunostaining and quantification of MVD from 3 and 5 month old *KPC* and *RGE-KPC* tumors also revealed significantly reduced MVD in *RGE-KPC* tumors (Fig. 3G-H and S4B-C). We also examined the MVD of *KIC* and *RGE-KIC* tissues at 1 month old. At this time point, more than 90% of the tissue retained amylase expression. There was no difference in MVD in amylase positive areas between *KIC* and *RGE-KIC* tissues (Fig. S5A-C). Additionally, pancreas tissue from

non-tumor bearing *WT* and *RGE* mice were analyzed for MVD (Fig. S5D). Again, no significant difference between the two groups was observed (Fig. S5E-F). We found that the number of proliferating endothelial cells co-stained with phospho-histone H3 and endomucin was decreased in tumors in *RGE* animals compared to tumors in *WT* mice, supporting the reduction of MVD in *RGE-KIC* and *RGE-KPC* tumors (Fig. 3I-M and S4D-E). Overall, the reduction of MVD correlated with tumor specific induction of ROS in *RGE* animals (Fig. 3A and S4A, 3B and S4B-C). These data suggest that the absence of functional Fbln5 impairs endothelial cell survival specifically in the tumor microenvironment.

Induction of the oxidative stress responsive gene Nqo1 by FN-induced ROS *in vitro* and *in vivo*

Our data suggested that Fbln5 controls ROS production through FN–β1 integrin interaction. To elucidate the underlying molecular mechanism of ROS generation, we isolated *WT*, *KO* and *RGE* primary MEFs. Fbln5 expression levels were equivalent between *WT* and *RGE* MEFs (Fig. S6). We found that ROS was elevated in *KO* and *RGE* MEFs but not in *WT* MEFs when cells were plated on FN (Fig. 4A). Next, we performed qPCR arrays to screen for oxidative stress and antioxidant response pathway related genes using RNA harvested from *WT* and *RGE* MEFs. From these arrays, NADP(H):quinone oxidoreductase 1 (Nqo1) was a reproducible and reliable target that was increased in *RGE* MEFs after plating on FN. Nqo1 is an antioxidant enzyme that is responsible for the reduction of quinones to hydroquinones utilizing NAD(P)H as an electron donor (25). Reducing quinone levels lowers the occurrence of ROS generation as a result of redox cycling (25). Induction of Nqo1 can be mediated by the Keap1/Nrf2/ARE pathway (26). The induction of Nqo1 in *RGE* MEFs when plated on FN was confirmed by quantitative real-time PCR (Fig. 4B), enzymatic activity (Fig. 4C) and Western blotting (Fig. 4D). Concordantly, the induction of Nqo1 expression was reversed by antioxidant treatment (with NAC) in a dose-dependent manner (Fig. 4E), showing that the elevation of Nqo1 is a consequence of increased ROS status in *RGE* MEFs. In addition, Nqo1 induction was elevated in tumors from *RGE* animals (Fig. 4F-G).

Nqo1 induction is dependent on FN-β1 integrin interaction and 5-lipooxygenase (5-Lox) activity

It has been reported that integrin activation by FN can induce ROS production (12). Accordingly, when the endothelial cell line bEnd.3 was treated with a α5β1 integrin-activating antibody, Nqo1 levels were induced (Fig. 5A). The induction of Nqo1 was specific to activation by FN and was not present when cells were plated on plastic or collagen (Fig. 5B). Induction was partially blocked by β1 integrin blockade (Fig. 5B). Given this data, we conclude that the induction of Nqo1 is responsive to ROS production induced by FN mediated β1 integrin ligation.

To determine the cellular source of ROS production in the absence of Fbln5-integrin interaction, we used inhibitors for various ROS sources including the mitochondrial respiratory chain inhibitor Rotenone, NADPH oxidase (NOX) inhibitor Diphenyleneiodonium chloride (DPI) and 5-lipoxygenase (5-Lox) inhibitor,

nordihydroguaiaretic acid (NDGA). Treatment with Rotenone or DPI did not suppress the induction of Nqo1, suggesting mitochondria and NOX are not the intracellular source of ROS production (Fig. 5C). In addition, there was no induction of NOX enzymatic activity in *RGE* MEFs compared to WT MEFs by FN (Fig. S7). In contrast, inhibition of 5-Lox by NDGA reduced Nqo1 levels, indicating 5-Lox as the potential source of ROS (Fig. 5D). The quantification results were shown in Fig. 5E. This is consistent with a previous discovery that 5-Lox contributes to a strong burst of ROS production by FN-integrin engagement (11).

ROS induction has an additive therapeutic effect when combined with standard chemotherapy agents and development of Fbln5 targeted agents

To determine if increased integrin-induced ROS improved response to chemotherapy we compared the efficacy of standard chemotherapy agents Gemcitabine (Gem) and Abraxane (Abx) in *KIC* and *RGE-KIC* mice. Due to poor diagnosis for pancreatic cancer, most patients received therapy in later stages. To mimic patient condition, all therapy started at 1.5 month old when both *KIC* and *RGE-KIC* mice have established solid tumors (Fig.S2C). We found that low-dose Gemcitabine (GemL) and Abx were more effective in the context of mutant Fbln5 (Fig. 6A-B). Survival studies were also performed with cohorts of *KIC* and *RGE-KIC* mice treated with GemL, high-dose Gemcitabine (GemH) and Abx. *RGE-KIC* mice consistently survived significantly longer in all three treatment groups than similarly treated *KIC* mice (Fig. 6C-E). These data suggest that increasing integrin-induced ROS augments the activity of standard chemotherapy.

Discussion

We demonstrated that Fbln5 expression is induced in a significant percentage of pancreatic cancers and that it promotes tumor progression by competing with FN for integrin ligation. Global loss of Fbln5-integrin interaction resulted in decreased tumor growth and prolonged survival of tumor-bearing mice with no apparent adverse effects in normal tissues. The decrease in tumor burden was dependent on increased FN-mediated integrin activation, which increased ROS production through 5-Lox activity and resulted in reduced angiogenesis in the tumor microenvironment. These findings are summarized in Figure 7.

The ECM provides a structural framework in which tumors develop and progress. ECM signaling contributes to cell survival, proliferation and migration, thus regulation of cellular events initiated by the ECM is critical for tumor progression. To date, pharmacologic modification of the ECM in PDA has not resulted in improvement of chemoresponse or overall survival in patients (27-29). However, preclinical studies focused on inhibiting pathways that stimulate ECM deposition (e.g., TGFβ) have shown promise in promoting tumor control (30). Here, we have highlighted that increased integrin activation can result in decreased tumor growth by elevating integrin-induced ROS production. The extent of cell-ECM interaction is regulated in part by matricellular proteins, including Fbln5. Yet, the contribution of Fbln5 to cancer has been limited largely to expression studies (31-34), which have not defined a clear function for Fbln5 in tumorigenesis. We found that FBLN5 protein was expressed in all of the human PDA samples (n=25) we evaluated. Expression was largely restricted to the stromal compartment, yet the pattern of expression was not uniform

as there were some areas of stroma that were negative or only weakly reactive. This heterogeneity suggests that evaluation of FBLN5 and potentially other matricellular proteins in human tissue microarrays could be challenging. Additional studies on the expression of Fbln5 protein in clinically annotated tumor samples are needed to elucidate if Fbln5 expression has predictive value.

To extend our studies, we sought to understand how Fbln5-integrin interaction functions in the context of the microenvironment of PDA. We employed two distinct but related GEMMs of PDA that recapitulate common mutations observed in the human disease (35-37). The expression of Fbln5 in each model is similar to the expression level and pattern of Fbln5 expression in human PDA. Furthermore, FN and α5β1 integrin are expressed abundantly in animal models of PDA as well as human PDA (38, 39). To study Fbln5-integrin interaction we took advantage of the fact that 1) Fbln5 binds but does not activate α5β1 (8, 14), suggesting that it can function to reduce binding of other ligands of the integrin; and 2) knockin mice carrying a point mutation in the integrin binding domain of Fbln5 (*RGE* mice) are viable and fertile (15). The described essential function of Fbln5 is in elastic fiber assembly as shown by Fbln5-deficient animals (17, 18) and biochemical analysis (16, 40). However, *RGE* mice have intact elastic fibers (15), indicating that Fbln5-integrin binding is not required for elastic fiber assembly. These data strongly suggest that the phenotype in the *RGE* animals is not due to changes in elastic fiber assembly but a result of an increase in integrin activation by ligands other than Fbln5. Given the dramatic increase in FN expression as well as other stromal components in PDA we postulated that the tumor microenvironment would provide a biologically meaningful stress to ascertain the functional consequences of increased integrin ligation in *RGE* animals.

ROS production as a result of integrin ligation is a well-established (11, 12), although underappreciated signalling pathway. Previously, we discovered that the loss of Fbln5-integrin interaction results in increased integrin-induced ROS production (13). Cellular redox homeostasis is tightly regulated by the balance between ROS scavenging and eliminating systems (19). Cancer cells often generate higher levels of ROS due to metabolic abnormality, activation of oncogenes or loss of functional p53 (19). For example, increased levels of ROS, particularly H_2O_2 are highly mutagenic and contribute to elevated mutation levels and heterogeneity. Thus an imbalance in ROS scavenging and eliminating systems is likely to result in acute consequences in the tumor microenvironment. For example, increasing ROS levels might result in inhibition of cell proliferation and ultimately cell death (41). However, cancer cells have developed adaptive mechanisms to manage increased ROS levels (19). One adaptive mechanism is the induction of the antioxidant response transcription factor Nrf2 to increase the expression of the ROS detoxification enzyme Nqo1 (42, 43). We found that the loss of Fbln5-integrin interaction induces Nqo1 and that this response is ROS-dependent. Nqo1 levels as a result further validated the elevation of oxidative stress in tumors grown in *RGE* mice and also provided a tractable biochemical endpoint to evaluate the signaling cascade induced by FN in the absence of integrin binding Fbln5. Furthermore, using Nqo1 levels as an endpoint, we discovered that ablation of Fbln5-integrin interaction increased 5-Lox activity in a FN-dependent manner. Pharmacologic inhibition of 5-Lox rescued the FN-driven phenotype *in vitro* implicating that 5-Lox is

downstream of integrin activation. This is consistent with previous reports showing that integrin activation by FN can stimulate ROS production primarily through 5-Lox (11, 12). FN has also been reported to stimulate intracellular ROS in pancreatic cancer cells through NOX and the mitochondria (10), although we did not find evidence of this in our system.

We found that stromal and tumor cells express the integrin profile required for FN-induced ROS production. However, changes in endothelial cells were the most apparent phenotype in tumors from *RGE* mice. Endothelial cells are sensitive to elevated ROS (44) and this was evident by the consistent reduction in microvessel density and reduction in proliferating endothelial cells in tumors grown in *RGE* animals. Fibroblasts from *RGE* mice produce elevated levels of ROS in culture in a FN and integrin-dependent manner. Yet, surprisingly, we found no significant changes in the presence or activation of fibroblasts in tumors from *RGE* mice (data not shown). Global analysis of ROS using DHE indicates that many cell types, including tumor cells, display elevated ROS levels in tumors from *RGE* mice. However, in vitro studies suggest that Fbln5 does not affect ECM-mediated ROS induction in tumor cells (data not shown). It is plausible that long lived ROS molecules (e.g., H_2O_2) travel from stromal cells and increase oxidative stress in tumor cells resulting in decreased proliferation and reduced tumor growth. It is also feasible that endothelial cells in the tumor microenvironment succumb to elevated ROS induced by mutant Fbln5 and the decreased tumor growth is akin to an anti-angiogenic effect. In contrast, Fbln5 null mice display an exaggerated vascular response after subcutaneous implantation of polyvinyl alcohol sponges (24). However, the mechanism of how Fbln5 directly affects endothelial cell function and the contribution of integrins in this phenotype is poorly understood. In our model, non-tumor bearing pancreata of *WT* and *RGE* mice show similar microvessel density (Fig. S5). However, in the context of the tumor microenvironment the basal level of ROS is increased compared to normal pancreas, therefore inducing further ROS by mutation of Fbln5 may explain the negative effect on endothelial cell function. If so, this suggests that the mutation in Fbln5 functions as an endogenous inhibitor of angiogenesis selectively in the tumor microenvironment. These hypotheses are currently being evaluated.

Our studies show that Fbln5 functions as a rheostat to dampen integrin-mediated ROS production. This function of reducing cell-ECM interaction is similar to what has been observed for other matricellular proteins. For example, SPARC reduces the binding of fibrillar collagens to discoidin domain receptors thereby reducing collagen induced cell signaling and attachment (1). Current studies are focused on understanding factors that drive Fbln5 expression in the tumor microenvironment and identification of the integrin-mediated signaling pathway that activates 5-Lox in the context of mutant Fbln5. Overall, our study illustrates how the matricellular protein Fbln5 functions to reduce FN-integrin interaction and suggests that Fbln5 is a novel therapeutic target for pancreatic cancer.

Supplementary Material

Refer to Web version on PubMed Central for supplementary material.

Acknowledgments

This work was supported in part by grants from the American Cancer Society (ACS, RSG-10-244-01-CSM to R.A.B.), The Joe and Jessie Crump Medical Research Foundation (to R.A.B.), NIH (R01 CA118240 to R.A.B., R01 CA137181 to D.H.C. and T32 GM008203 to M. T.), the Effie Marie Cain Scholarship in Angiogenesis Research (to R.A.B.) and Remeditex Ventures. The UT Southwestern Tissue Resource is supported by the NCI (5P30 CA142543). The funders had no role in study design, data collection, data analysis, decision to publish, or preparation of the manuscript. We acknowledge helpful discussions with Drs. Michael Dellinger and Adi Gazdar and members of the Brekken laboratory.

References

1. Aguilera KY, Rivera LB, Hur H, Carbon JG, Toombs JE, Goldstein CD, et al. Collagen signaling enhances tumor progression after anti-VEGF therapy in a murine model of pancreatic ductal adenocarcinoma. Cancer Res. 2014; 74:1032–44. [PubMed: 24346431]
2. Aoudjit F, Vuori K. Integrin signaling in cancer cell survival and chemoresistance. Chemother Res Pract. 2012; 2012:283181. [PubMed: 22567280]
3. Mantoni TS, Lunardi S, Al-Assar O, Masamune A, Brunner TB. Pancreatic stellate cells radioprotect pancreatic cancer cells through beta1-integrin signaling. Cancer Res. 2011; 71:3453–8. [PubMed: 21558392]
4. Sebens Muerkoster S, Kotteritzsch J, Geismann C, Gast D, Kruse ML, Altevogt P, et al. alpha5-integrin is crucial for L1CAM-mediated chemoresistance in pancreatic adenocarcinoma. International journal of oncology. 2009; 34:243–53. [PubMed: 19082495]
5. Sethi T, Rintoul RC, Moore SM, MacKinnon AC, Salter D, Choo C, et al. Extracellular matrix proteins protect small cell lung cancer cells against apoptosis: a mechanism for small cell lung cancer growth and drug resistance in vivo. Nature medicine. 1999; 5:662–8.
6. Meredith JE Jr, Fazeli B, Schwartz MA. The extracellular matrix as a cell survival factor. Molecular biology of the cell. 1993; 4:953–61. [PubMed: 8257797]
7. Maitra A, Hruban RH. Pancreatic cancer. Annu Rev Pathol. 2008; 3:157–88. [PubMed: 18039136]
8. Lomas AC, Mellody KT, Freeman LJ, Bax DV, Shuttleworth CA, Kielty CM. Fibulin-5 binds human smooth-muscle cells through alpha5beta1 and alpha4beta1 integrins, but does not support receptor activation. Biochem J. 2007; 405:417–28. [PubMed: 17472576]
9. Wong GS, Rustgi AK. Matricellular proteins: priming the tumour microenvironment for cancer development and metastasis. Br J Cancer. 2013; 108:755–61. [PubMed: 23322204]
10. Edderkaoui M, Hong P, Vaquero EC, Lee JK, Fischer L, Friess H, et al. Extracellular matrix stimulates reactive oxygen species production and increases pancreatic cancer cell survival through 5-lipoxygenase and NADPH oxidase. Am J Physiol Gastrointest Liver Physiol. 2005; 289:G1137–47. [PubMed: 16037546]
11. Taddei ML, Parri M, Mello T, Catalano A, Levine AD, Raugei G, et al. Integrin-mediated cell adhesion and spreading engage different sources of reactive oxygen species. Antioxid Redox Signal. 2007; 9:469–81. [PubMed: 17280488]
12. Chiarugi P, Pani G, Giannoni E, Taddei L, Colavitti R, Raugei G, et al. Reactive oxygen species as essential mediators of cell adhesion: the oxidative inhibition of a FAK tyrosine phosphatase is required for cell adhesion. J Cell Biol. 2003; 161:933–44. [PubMed: 12796479]
13. Schluterman MK, Chapman SL, Korpanty G, Ozumi K, Fukai T, Yanagisawa H, et al. Loss of fibulin-5 binding to beta1 integrins inhibits tumor growth by increasing the level of ROS. Dis Model Mech. 2010; 3:333–42. [PubMed: 20197418]
14. Nakamura T, Ruiz-Lozano P, Lindner V, Yabe D, Taniwaki M, Furukawa Y, et al. DANCE, a novel secreted RGD protein expressed in developing, atherosclerotic, and balloon-injured arteries. J Biol Chem. 1999; 274:22476–83. [PubMed: 10428823]
15. Budatha M, Roshanravan S, Zheng Q, Weislander C, Chapman SL, Davis EC, et al. Extracellular matrix proteases contribute to progression of pelvic organ prolapse in mice and humans. J Clin Invest. 2011; 121:2048–59. [PubMed: 21519142]

16. Zheng Q, Davis EC, Richardson JA, Starcher BC, Li T, Gerard RD, et al. Molecular analysis of fibulin-5 function during de novo synthesis of elastic fibers. Mol Cell Biol. 2007; 27:1083–95. [PubMed: 17130242]
17. Yanagisawa H, Davis EC, Starcher BC, Ouchi T, Yanagisawa M, Richardson JA, et al. Fibulin-5 is an elastin-binding protein essential for elastic fibre development in vivo. Nature. 2002; 415:168–71. [PubMed: 11805834]
18. Nakamura T, Lozano PR, Ikeda Y, Iwanaga Y, Hinek A, Minamisawa S, et al. Fibulin-5/DANCE is essential for elastogenesis in vivo. Nature. 2002; 415:171–5. [PubMed: 11805835]
19. Trachootham D, Alexandre J, Huang P. Targeting cancer cells by ROS-mediated mechanisms: a radical therapeutic approach? Nat Rev Drug Discov. 2009; 8:579–91. [PubMed: 19478820]
20. Kawaguchi Y, Cooper B, Gannon M, Ray M, MacDonald RJ, Wright CV. The role of the transcriptional regulator Ptf1a in converting intestinal to pancreatic progenitors. Nat Genet. 2002; 32:128–34. [PubMed: 12185368]
21. Aguirre AJ, Bardeesy N, Sinha M, Lopez L, Tuveson DA, Horner J, et al. Activated Kras and Ink4a/Arf deficiency cooperate to produce metastatic pancreatic ductal adenocarcinoma. Genes Dev. 2003; 17:3112–26. [PubMed: 14681207]
22. Hingorani SR, Wang L, Multani AS, Combs C, Deramaudt TB, Hruban RH, et al. Trp53R172H and KrasG12D cooperate to promote chromosomal instability and widely metastatic pancreatic ductal adenocarcinoma in mice. Cancer Cell. 2005; 7:469–83. [PubMed: 15894267]
23. Mah LJ, El-Osta A, Karagiannis TC. gammaH2AX: a sensitive molecular marker of DNA damage and repair. Leukemia. 2010; 24:679–86. [PubMed: 20130602]
24. Sullivan KM, Bissonnette R, Yanagisawa H, Hussain SN, Davis EC. Fibulin-5 functions as an endogenous angiogenesis inhibitor. Lab Invest. 2007; 87:818–27. [PubMed: 17607303]
25. Siegel D, Gustafson DL, Dehn DL, Han JY, Boonchoong P, Berliner LJ, et al. NAD(P)H:quinone oxidoreductase 1: role as a superoxide scavenger. Mol Pharmacol. 2004; 65:1238–47. [PubMed: 15102952]
26. Lee JM, Calkins MJ, Chan K, Kan YW, Johnson JA. Identification of the NF-E2-related factor-2-dependent genes conferring protection against oxidative stress in primary cortical astrocytes using oligonucleotide microarray analysis. J Biol Chem. 2003; 278:12029–38. [PubMed: 12556532]
27. Lee JJ, Perera RM, Wang H, Wu DC, Liu XS, Han S, et al. Stromal response to Hedgehog signaling restrains pancreatic cancer progression. Proceedings of the National Academy of Sciences. 2014; 111:E3091–E100.
28. Rhim, Andrew D.; Oberstein, Paul E.; Thomas, Dafydd H.; Mirek, Emily T.; Palermo, Carmine F.; Sastra, Stephen A., et al. Stromal Elements Act to Restrain, Rather Than Support, Pancreatic Ductal Adenocarcinoma. Cancer Cell. 2014; 25:735–47. [PubMed: 24856585]
29. Provenzano, Paolo P.; Cuevas, C.; Chang, Amy E.; Goel, Vikas K.; Von Hoff, Daniel D.; Hingorani, Sunil R. Enzymatic Targeting of the Stroma Ablates Physical Barriers to Treatment of Pancreatic Ductal Adenocarcinoma. Cancer Cell. 21:418–29. [PubMed: 22439937]
30. Ostapoff KT, Kutluk Cenik B, Wang M, Ye R, Xu X, Nugent D, et al. Neutralizing murine TGFβR2 promotes a differentiated tumor cell phenotype and inhibits pancreatic cancer metastasis. Cancer Research. 2014
31. Yue W, Sun Q, Landreneau R, Wu C, Siegfried JM, Yu J, et al. Fibulin-5 suppresses lung cancer invasion by inhibiting matrix metalloproteinase-7 expression. Cancer Res. 2009; 69:6339–46. [PubMed: 19584278]
32. Lee YH, Albig AR, Regner M, Schiemann BJ, Schiemann WP. Fibulin-5 initiates epithelial-mesenchymal transition (EMT) and enhances EMT induced by TGF-beta in mammary epithelial cells via a MMP-dependent mechanism. Carcinogenesis. 2008; 29:2243–51. [PubMed: 18713838]
33. Hu Z, Ai Q, Xu H, Ma X, Li HZ, Shi TP, et al. Fibulin-5 is down-regulated in urothelial carcinoma of bladder and inhibits growth and invasion of human bladder cancer cell line 5637. Urol Oncol. 2011; 29:430–5. [PubMed: 19767220]
34. Wang Q, Li XG, Zhang Y, Cao LQ, Deng ZH, Chen Y. Expression of EVEC in ovarian carcinoma and its biological significance. Zhonghua Zhong Liu Za Zhi. 2010; 32:676–80. [PubMed: 21122382]

35. Olive KP, Jacobetz MA, Davidson CJ, Gopinathan A, McIntyre D, Honess D, et al. Inhibition of Hedgehog signaling enhances delivery of chemotherapy in a mouse model of pancreatic cancer. Science. 2009; 324:1457–61. [PubMed: 19460966]
36. Singh M, Ferrara N. Modeling and predicting clinical efficacy for drugs targeting the tumor milieu. Nat Biotechnol. 2012; 30:648–57. [PubMed: 22781694]
37. Olive KP, Tuveson DA. The use of targeted mouse models for preclinical testing of novel cancer therapeutics. Clin Cancer Res. 2006; 12:5277–87. [PubMed: 17000660]
38. Ansari D, Aronsson L, Sasor A, Welinder C, Rezeli M, Marko-Varga G, et al. The role of quantitative mass spectrometry in the discovery of pancreatic cancer biomarkers for translational science. Journal of translational medicine. 2014; 12:87. [PubMed: 24708694]
39. Jagadeeshan S, Krishnamoorthy YR, Singhal M, Subramanian A, Mavuluri J, Lakshmi A, et al. Transcriptional regulation of fibronectin by p21-activated kinase-1 modulates pancreatic tumorigenesis. Oncogene. 2014
40. Hirai M, Ohbayashi T, Horiguchi M, Okawa K, Hagiwara A, Chien KR, et al. Fibulin-5/DANCE has an elastogenic organizer activity that is abrogated by proteolytic cleavage in vivo. J Cell Biol. 2007; 176:1061–71. [PubMed: 17371835]
41. Kardeh S, Ashkani-Esfahani S, Alizadeh AM. Paradoxical action of reactive oxygen species in creation and therapy of cancer. Eur J Pharmacol. 2014; 735C:150–68. [PubMed: 24780648]
42. Awadallah NS, Dehn D, Shah RJ, Russell Nash S, Chen YK, Ross D, et al. NQO1 expression in pancreatic cancer and its potential use as a biomarker. Appl Immunohistochem Mol Morphol. 2008; 16:24–31. [PubMed: 18091324]
43. DeNicola GM, Karreth FA, Humpton TJ, Gopinathan A, Wei C, Frese K, et al. Oncogene-induced Nrf2 transcription promotes ROS detoxification and tumorigenesis. Nature. 2011; 475:106–9. [PubMed: 21734707]
44. Kietadisorn R, Juni RP, Moens AL. Tackling endothelial dysfunction by modulating NOS uncoupling: new insights into its pathogenesis and therapeutic possibilities. American journal of physiology Endocrinology and metabolism. 2012; 302:E481–95. [PubMed: 22167522]
45. Dineen SP, Roland CL, Greer R, Carbon JG, Toombs JE, Gupta P, et al. Smac mimetic increases chemotherapy response and improves survival in mice with pancreatic cancer. Cancer Res. 2010; 70:2852–61. [PubMed: 20332237]
46. Ostapoff KT, Awasthi N, Cenik BK, Hinz S, Dredge K, Schwarz RE, et al. PG545, an angiogenesis and heparanase inhibitor, reduces primary tumor growth and metastasis in experimental pancreatic cancer. Mol Cancer Ther. 2013; 12:1190–201. [PubMed: 23696215]
47. Hallmann R, Mayer DN, Berg EL, Broermann R, Butcher EC. Novel mouse endothelial cell surface marker is suppressed during differentiation of the blood brain barrier. Dev Dyn. 1995; 202:325–32. [PubMed: 7626790]
48. Weng S, Wang H, Chen W, Katz MH, Chatterjee D, Lee JE, et al. Overexpression of protein phosphatase 4 correlates with poor prognosis in patients with stage II pancreatic ductal adenocarcinoma. Cancer epidemiology, biomarkers & prevention: a publication of the American Association for Cancer Research, cosponsored by the American Society of Preventive Oncology. 2012; 21:1336–43.
49. Ye R, Jung DY, Jun JY, Li J, Luo S, Ko HJ, et al. Grp78 heterozygosity promotes adaptive unfolded protein response and attenuates diet-induced obesity and insulin resistance. Diabetes. 2010; 59:6–16. [PubMed: 19808896]
50. Rivera LB, Brekken RA. SPARC promotes pericyte recruitment via inhibition of endoglin-dependent TGF-beta1 activity. J Cell Biol. 2011; 193:1305–19. [PubMed: 21708981]
51. Pink JJ, Planchon SM, Tagliarino C, Varnes ME, Siegel D, Boothman DA. NAD(P)H:Quinone oxidoreductase activity is the principal determinant of beta-lapachone cytotoxicity. J Biol Chem. 2000; 275:5416–24. [PubMed: 10681517]
52. Fitzsimmons SA, Workman P, Grever M, Paull K, Camalier R, Lewis AD. Reductase enzyme expression across the National Cancer Institute Tumor cell line panel: correlation with sensitivity to mitomycin C and EO9. J Natl Cancer Inst. 1996; 88:259–69. [PubMed: 8614004]

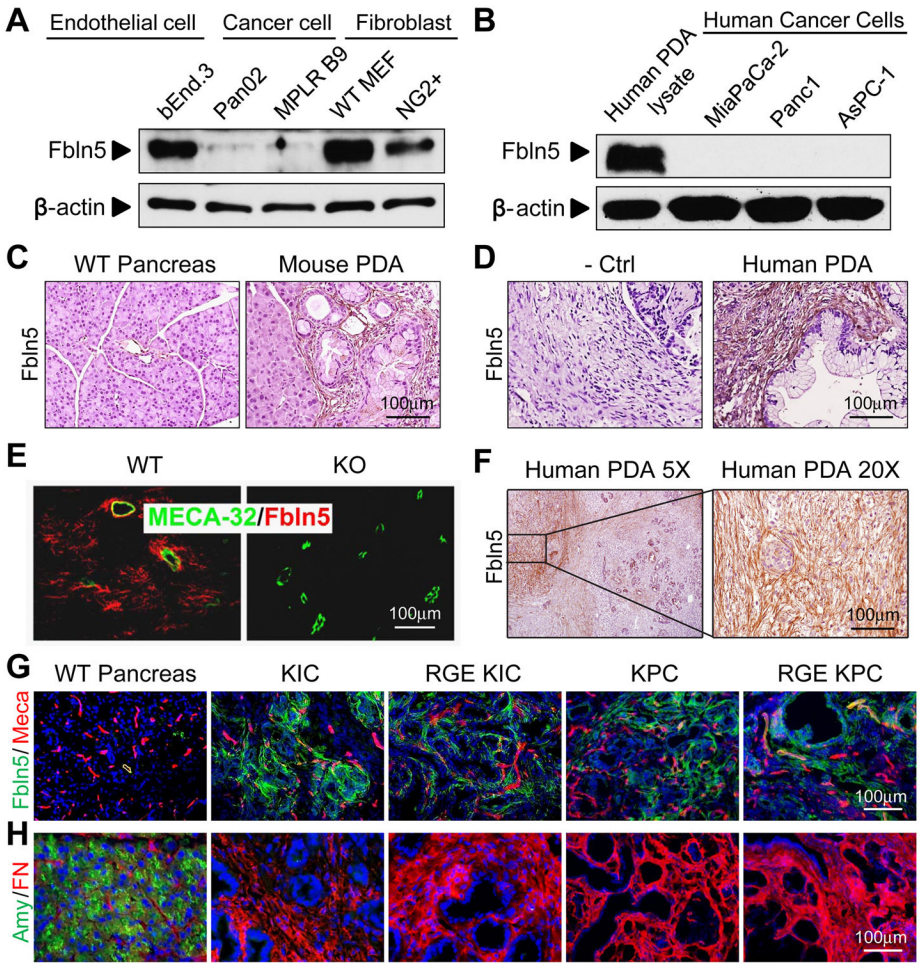

Figure 1. Expression pattern of Fbln5 in mouse and human

(A-B) Protein lysates from mouse endothelial cells, cancer cells and fibroblasts (A) and human PDA tissue and cancer cell lines (B) were probed for indicated targets by Western blot. (C-D) Immunohistochemical (IHC) staining for Fbln5 on mouse (C) and human (D) PDA sections. (E) Immunofluorescence (IF) staining of Fbln5 (Red) and MECA-32 (Green) on subcutaneously grown pancreatic tumor (Pan02) in Fbln5 *WT* and *KO* mice. (F) Representative images of FBLN5 expression in human PDA, showing heterogeneous expression in the stroma. (G-H) Immunofluorescence (IF) staining of *WT* pancreas, *KIC* and *RGE KIC* tumors, *KPC* and *RGE KPC* tumors for Fbln5 (green) and endothelial cell marker Meca32 (Meca) (red) in panel (G), acinar cell marker amylase (Amy) (green) and FN (red) in panel (H). Nucleuses were counterstained with DAPI (blue). Scale bars are presented as indicated.

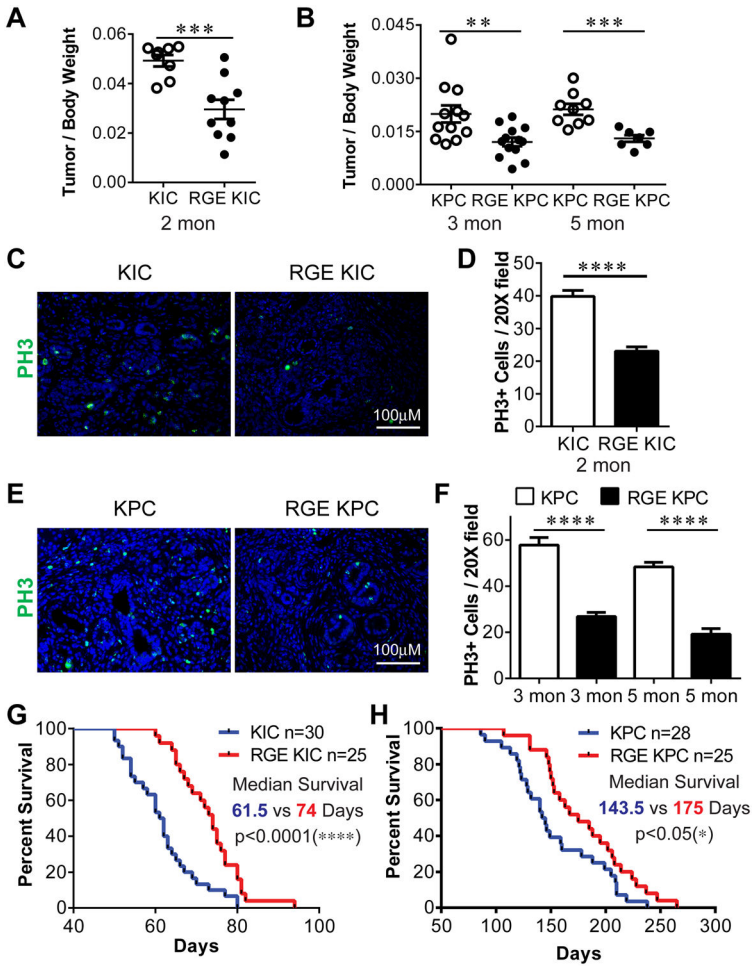

Figure 2. *RGE KIC* and *RGE KPC* mice show reduced tumor growth and prolonged survival compared to *KIC and KPC* mice

(A-B) Whole tumors were isolated and weighed and normalized against body weight at 2 months for *KIC* and *RGE KIC* mice (A) or 3 and 5 months for *KPC* and *RGE KPC* mice (B). n≥7 tumors per group. (C, E) IF staining on tumor sections for phospho-Histone H3 (PH3) (green). n≥4 tumors per group. (D, F) Quantification of PH3 positive (+) cells per 20× field from 4-5 tumors per group with 8-10 pictures per tumor. Results are shown as mean±s.e.m. (G-H) Kaplan-Meier survival curve of *KIC* and *RGE KIC* mice (G), *KPC* and *RGE KPC* mice (H). Scale bars are presented as indicated. For statistical analysis, unpaired t test was used for panel (A), (B), (D) and (F). Log-rank test was used for panel (G) and (H). *, p<0.05, **, p<0.01, ***, p<0.001, ****, p<0.0001.

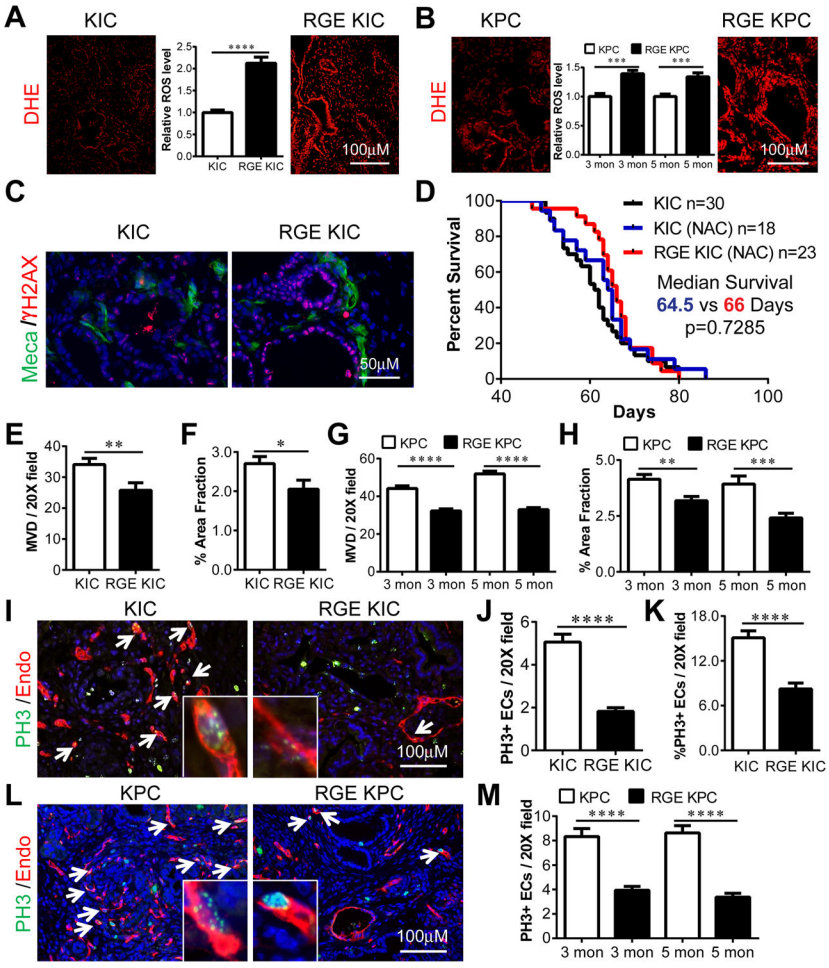

Figure 3. Increased oxidative stress and reduced microvessel density (MVD) and endothelial cell (EC) proliferation in *RGE KIC* and *RGE KPC* tumors compared to *KIC* and *KPC* tumors

(A-B) Dihydroethidium (DHE) (red) staining on freshly cut frozen sections of *KIC* and *RGE KIC* (A), *KPC* and *RGE KPC* (B) tumors for *in situ* detection of ROS. Relative ROS level was quantified by fluorescence intensity using the software NIS-Elements and shown inside images. Quantification was from 3 tumors per group with 6-10 images per tumor. (C) IF staining on *KIC* and *RGE KIC* tumor sections for Meca32 (Meca) (green) and γ-H2AX (red). n=3 tumors per group. (D) Kaplan-Meier survival curve of *KIC* and *RGE KIC* mice treated with the antioxidant N-acetyl-Cysteine (NAC) by drinking water starting at 4 weeks old. (E, G) MVD was counted per 20× field from 4-5 *KIC* and *RGE KIC* (E), *KPC* and *RGE KPC* (G) tumors with 8-10 pictures per tumor. (F, H) Quantification of MVD for *KIC* and *RGE KIC* (F), *KPC* and *RGE KPC* (H) tumors using the software NIS-Elements. Endomucin (Endo) stained areas are counted as % area fraction. (I, L) IF staining on 2 month old *KIC* and *RGE KIC* (I) and 3 month old *KPC* and *RGE KPC* (L) tumor sections for PH3 (green) and Endo (red). Arrows indicate double labeled ECs, one of which was enlarged and shown in an insert box for each image. (J, M) Quantification of PH3 and Endo co-stained cells (PH3+ ECs) per 20× field in *KIC* and *RGE KIC* (J) and *KPC* and *RGE KPC* (M) tumors at indicated ages. (K) Quantification of % PH3+ ECs over total number of ECs in 20× field in *KIC* and *RGE KIC* tumors. Scale bars are presented as indicated. All the results shown are

mean±s.e.m. For statistical analysis, unpaired t test was used for panel (E-H), (J-K) and (M). *, $p<0.05$, **, $p<0.01$, ***, $p<0.001$ ****, $p<0.0001$.

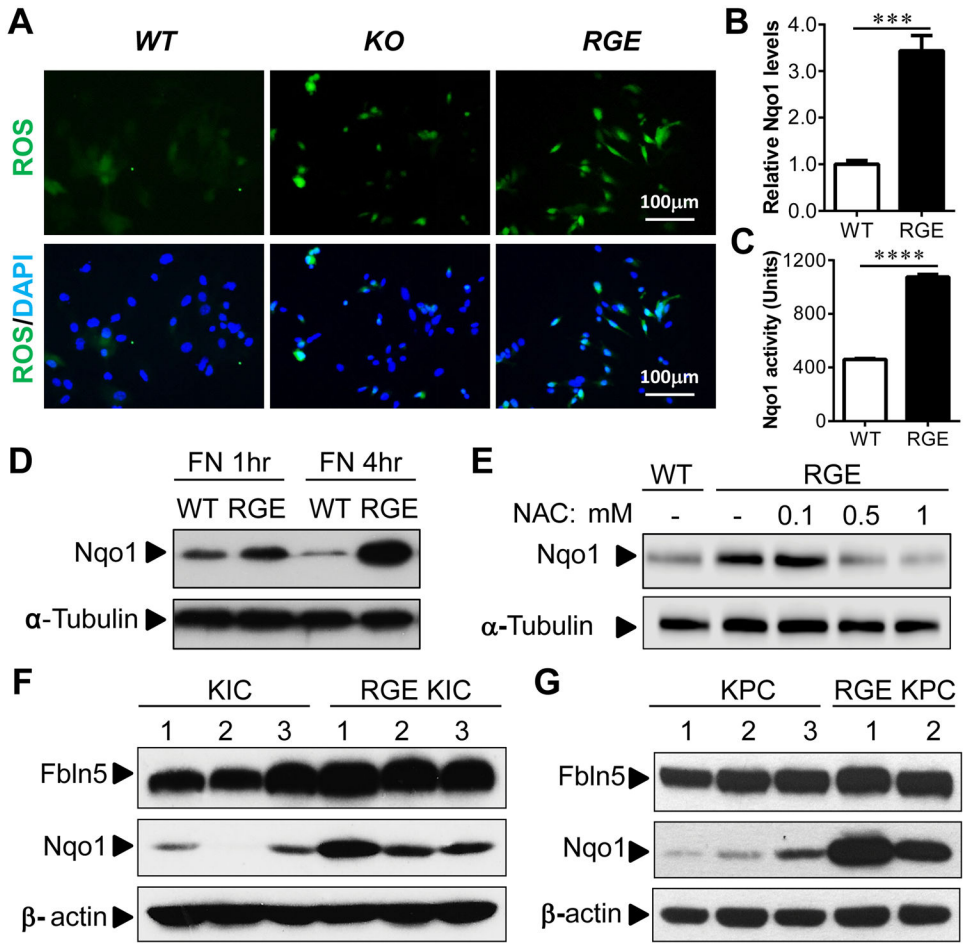

Figure 4. Fbln5 *RGE* mutation induces ROS production and oxidative stress responsive protein Nqo1 *in vitro* and *in vivo*

(A) MEFs harvested from *Fbln5 WT*, *KO* and *RGE* mice were grown on FN for 16hr and stained with DCF-DA (green) to detect ROS. Nucleus was counterstained in blue with DAPI. (B) Real time PCR result with RNA isolated from *WT* or *RGE* MEFs plated on FN for 24hr. (C) Enzymatic activity of Nqo1 was measured and normalized against protein concentration with samples isolated from *WT* or *RGE* MEFs plated on FN for 4hr. (D) Western blot using lysates harvested from *WT* or *RGE* MEFs plated on FN for 1 or 4hr. (E) Western blot using lysates harvested from *WT* or *RGE* MEFs plated on FN for 4hrs and treated with increasing concentration of antioxidant N-acetyl cysteine (NAC). (F, G) Western blot using lysates harvested from several randomly selected *KIC* and *RGE KIC* tumors (F) or *KPC* and *RGE KPC* tumors (G). α-tubulin or β-actin was used as loading control. Scale bars are presented as indicated. All the results in (B) and (C) are mean±s.e.m. For statistical analysis, unpaired t test was used for panel (B) and (C). ***, $p<0.001$, ****, $p<0.0001$.

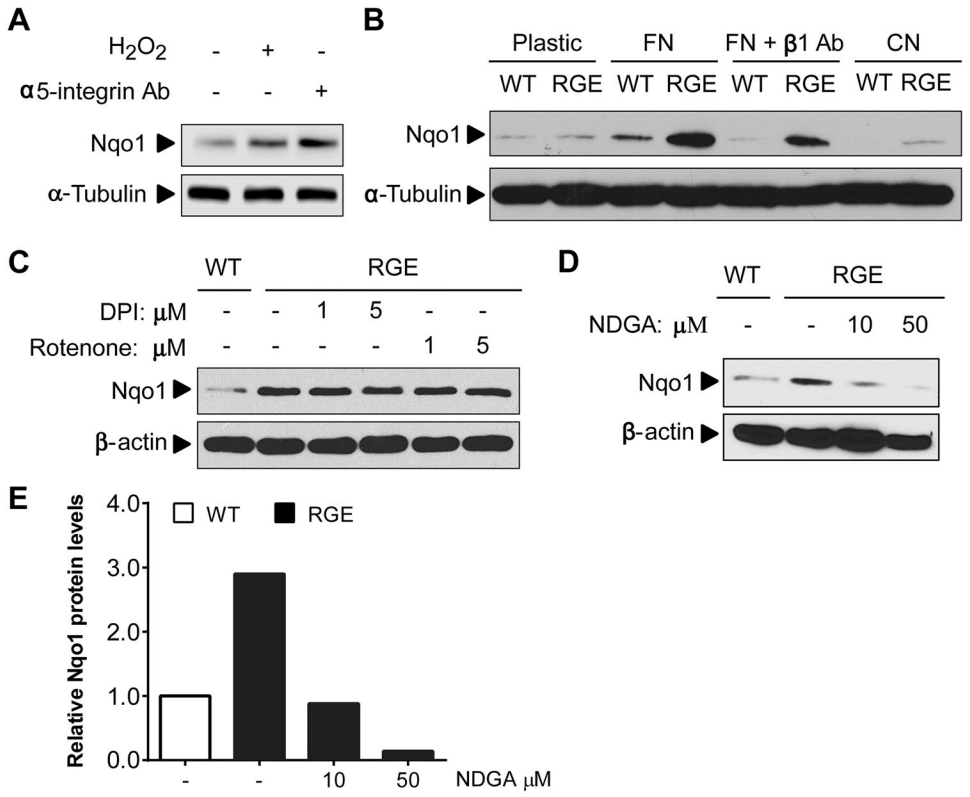

Figure 5. 5-LOX activation through FN-integrin interaction is responsible for ROS induction in *RGE* MEFs

(A) bEnd.3 cells were plated on FN for 4 hr and treated with 100 μM H_2O_2 or 10 μg/ml α5 integrin activating antibody at time of plating and probed for Nqo1 by Western blot. (B) *WT* or *RGE* MEFs were plated on plastic, FN, FN + β1 integrin blocking antibody (10 μg/ml) or Collagen (CN) for 4 hr. Lysates were then harvested and subjected to Western blot. (C) *RGE* MEFs were plated on FN and treated with the NADPH Oxidase (NOX) inhibitor DPI or the mitochondrial electron transport chain inhibitor Rotenone at the time of plating. Lysates were harvested after 4 hrs for Western blot. (D) *RGE* MEFs were plated on FN and treated with a 5-lipoxygenase (5-LOX) inhibitor (NDGA) at the time of plating and harvested 4 hrs later for Western blot. (E) Quantification results of relative Nqo1 protein levels from panel (D) using the software Image Studio Digits. α-tubulin or β-actin was used as loading control for all the Western blots.

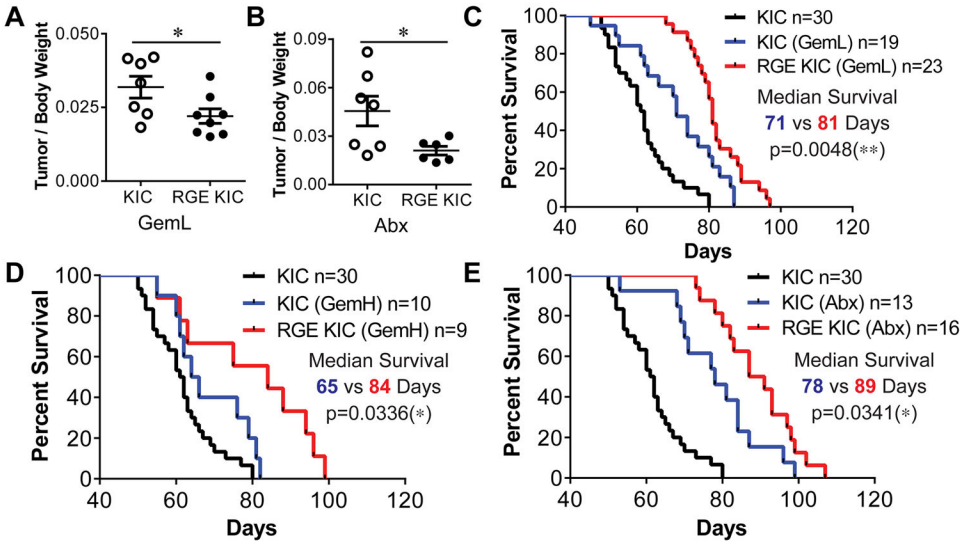

Figure 6. *RGE KIC* mice have increased survival compared to *KIC* mice when given chemotherapy

(A, B) *KIC* and *RGE KIC* mice were treated with 12.5 mg/kg Gemcitabine (Gem) 3×/wk (GemL) (A) or 5 mg/kg Abraxane (Abx) 2×/wk (B) for 3 wks starting at 7 week old. Mice were then sacrificed and tissues were isolated for analysis. Tumor size is presented as the mean ratio of tumor/body weight ±s.e.m. n≥6 tumors per group. (C-E) Kaplan-Meier survival curve of *KIC* control, *KIC* and *RGE KIC* mice treated with GemL (C), GemH (D) or Abx (E). All therapies were given to mice from 7 week old until moribund. For GemL, 12.5 mg/kg Gem was given to mice 3×/wk by intraperitoneal (i.p.) injection. For GemH, 50 mg/kg Gem was given to mice 1×/wk by i.p. injection. For Abx, 5 mg/kg was given to mice 2×/wk by i.p. injection. For statistical analysis, unpaired t test was used for panel (A-B). Log-rank test was used for panel (C-E). *, $p<0.05$, **, $p<0.01$.

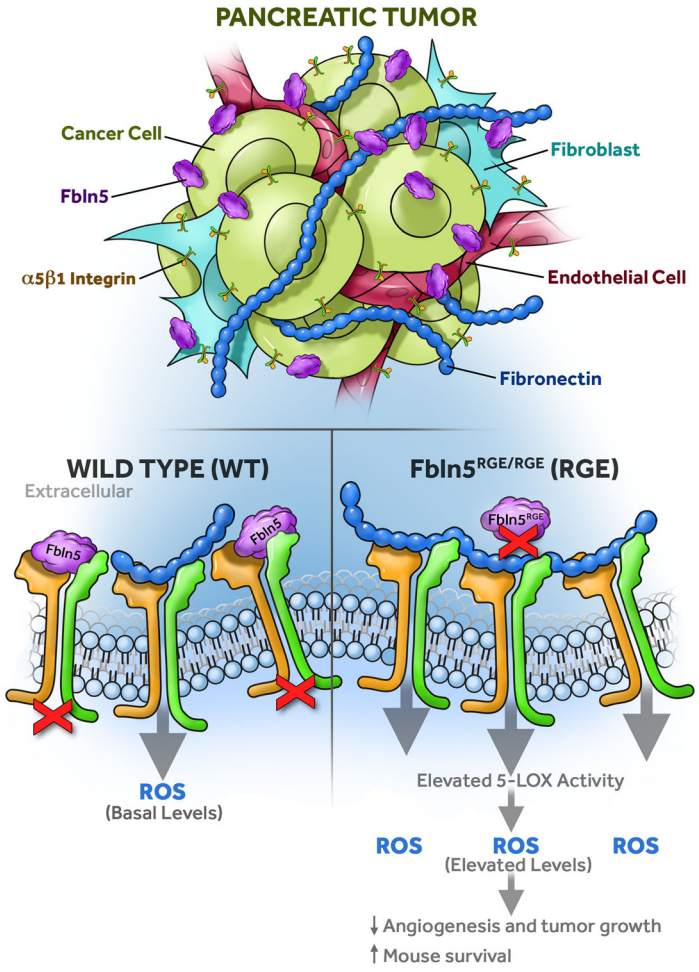

Figure 7. Fbln5 controls ROS production in the tumor microenvironment

Fbln5 is mainly secreted into the tumor microenvironment by tumor-associated fibroblasts (TAFs) and ECs. Fbln5 competes with FN for integrin binding. In the absence of Fbln5-integrin interaction (*RGE*), more FN will bind to integrin receptors and increase ROS production, resulting in increased 5-LOX activity and reduced angiogenesis and tumor growth.